International Journal of Heat and Mass Transfer 243 (2025) 126851

Contents lists available at ScienceDirect

International Journal of Heat and Mass Transfer

journal homepage: www.elsevier.com/locate/hmt

Assessment of the Oberbeck–Boussinesq approximation for buoyancy-driven turbulence in air

A. Cimarelli [a,*], A. Fenzi [a], D. Angeli [b], E. Stalio [a]

[a] DIEF, University of Modena and Reggio Emilia, Modena, 41125, Italy
[b] DISMI, University of Modena and Reggio Emilia, Reggio Emilia, 41122, Italy

ARTICLE INFO

Keywords:
Thermal turbulence
Rayleigh–Bénard convection
Oberbeck–Boussinesq approximation

ABSTRACT

The full mathematical representation of natural convection is very complex, as it involves, besides continuity and the equations for the transport of momentum and energy, one state equation for density and three laws for the dependency of the thermophysical parameters on pressure and temperature. In addition it requires the representation of pressure work and viscous dissipation in the energy equation. Most numerical simulations and theoretical studies of natural convection use a simplified model based on the Oberbeck–Boussinesq approximation. With respect to the general formulation, the simplified problem is characterized by a divergence-free velocity field, uses constant thermophysical parameters and neglects viscous dissipation and pressure work. Although the Oberbeck–Boussinesq equations have become a physical case in themselves, in certain flow conditions non-Oberbeck–Boussinesq phenomena are non-negligible thus significantly affecting the flow solution. The aim of the present work is to quantitatively identify the flow conditions that give rise to non-negligible non-Oberbeck–Boussinesq phenomena. We demonstrate that the use of direct numerical simulation data combined with the theoretical framework provided by Gray and Giorgini (1976) represents a sound practice to address this issue. The test-case selected is the Rayleigh–Bénard problem at Ra= 0.7×10^6 with air as working fluid. Direct numerical simulations carried out using the compressible, variable property formulation and the Oberbeck–Boussinesq approximation highlight that a 5% tolerance on variations of the thermophysical properties of air around the reference state $(\tilde{\Theta}_0, \tilde{P}_0)$ = (30 °C, 1 atm) only marginally affects the statistical values of both global and local quantities. However, this tolerance represents a very stringent condition that for a tank of height $\tilde{H} = 2$ m filled with air at a reference state $(\tilde{\Theta}_0, \tilde{P}_0)$ = (30 °C, 1 atm) leads to a rather low maximum Rayleigh number of the order of 10^{10} that can be investigated without considering the influence of non-Oberbeck–Boussinesq effects. Hence, some doubts about the use of the Oberbeck–Boussinesq approximation for the study of high Rayleigh numbers are envisaged at least for air as working fluid.

1. Introduction

Thermally driven turbulence is a rich multi-physics problem involving heat transfer and fluid mechanics where buoyancy effects are given by density variations with temperature and pressure. The first methodical set of observations on natural convection was carried out by Henri Bénard at the university of Paris and reported in the publication "Les tourbillons cellulaires dans une nappe liquide", published in the first days of January, 1901. Since then, a large number of studies have been published, aiming at sharing improved knowledge on these phenomena. In present days, thermal convection studies can be carried out theoretically, experimentally or numerically. As compared to experiments, numerical investigations provide a complete spatial and temporal representation of the phenomenon.

In simulations where buoyancy effects are taken in full consideration, density is a function of both temperature and pressure $\tilde{\rho} = \tilde{\rho}(\tilde{p}, \tilde{\Theta})$ and the same dependency holds for viscosity $\tilde{\mu}$, specific heat $\tilde{c}_p$ and thermal conductivity $\tilde{\lambda}$. Also pressure work and viscous dissipation are accounted for. However, the variable properties approach requires the use of specific numerical methods which can be both expensive numerically and prone to instabilities. Another possible approach, to be applied in cases where pressure effects are regarded as less important, is the low-Mach number approximation. Within the low-Mach number approach, density and the other parameters depend on temperature only.

In the Oberbeck–Boussinesq approximation, density is considered constant in all terms of the momentum and internal energy equations

* Corresponding author.
E-mail address: andrea.cimarelli@unimore.it (A. Cimarelli).

https://doi.org/10.1016/j.ijheatmasstransfer.2025.126851
Received 14 August 2024; Received in revised form 20 January 2025; Accepted 15 February 2025
Available online 6 March 2025

except for the source term of momentum $\tilde{\rho}\tilde{g}_i$, which accounts for the effects of gravity. The source of momentum is linearized about a reference temperature $\tilde{\rho}\tilde{g}_i = \tilde{\rho}_0\left[1-\tilde{\alpha}_0\left(\tilde{\Theta}-\tilde{\Theta}_0\right)\right]\tilde{g}_i$. Gravity is the single term in the momentum equations which sets a two-way coupling between the velocity field and temperature. The resulting flow is divergence-free and this makes the mathematical problem more easily amenable to numerical solution. In the Oberbeck–Boussinesq approximation $\tilde{\mu}$, $\tilde{c}_p$, $\tilde{\lambda}$ and the isobaric expansion coefficient $\tilde{\alpha}$ are kept constant; pressure work and viscous dissipation are neglected.

Aside from physical inconsistencies derived from the hypothesis of negligible pressure work [1,2] and viscous dissipation, the Oberbeck–Boussinesq approximation will inevitably lead to errors. Limits of applicability for natural convection cases are investigated in detail in the work by Gray and Giorgini [3]. Depending on the selection of the characteristic scales, their approach is applicable to natural convection in different configurations like horizontal layers or vertical plates. In their theory, fluid properties are assumed to vary with temperature and pressure. Linear expressions for the fluid properties are substituted in the governing equations and the result is made non-dimensional. This allows to recover the Oberbeck–Boussinesq model under the hypotheses of a number of parameters being small. Finally, each of such hypotheses is reconsidered to obtain the range of dimensional parameters which ensures validity of the Oberbeck–Boussinesq approximation. Deviations from the Oberbeck–Boussinesq model depend upon the properties of the working fluid and the specific case investigated, including vertical size of the domain, range of temperatures and reference pressure $\tilde{P}_0$ and temperature $\tilde{\Theta}_0$. The theory by Gray and Giorgini [3] is not accompanied by an assessment of typical errors affecting global quantities like the Nusselt number or first and second order statistics of the velocity or temperature fields in canonical, natural convection cases.

A number of studies are found in the literature, which discuss the effects of variable properties on different natural convection configurations. The early study by Zhong et al. [4] considers a differentially heat cavity in laminar conditions. Convection close to vertical walls is considered by Hernández and Zamora [5],Morrone and Campo [6]. A fairly large body of literature discusses the effects of non-Oberbeck-Boussinesq in Rayleigh-Bénard convection. Given that results also depend on the fluid employed, Rayleigh-Bénard works can be classified in studies using SF6 as a gas close to its critical point [7], ethane [8,9]; and cryogenic Helium [10].

A number of works have attempted to distinguish between non-Oberbeck-Boussinesq effects and the transition to the ultimate regime as possible causes for a sudden change – measured by Ahlers et al. [11] – in the scaling of Nusselt at high Rayleigh numbers. Direct numerical simulation of Rayleigh–Bènard convection in glycerol (Pr = 2548) using temperature-dependent thermophysical properties is carried out by Horn et al. [12]. The Oberbeck–Boussinesq model assumptions are not met for glycerol at ambient conditions. Simulations including variable coefficients show a remarkable breakdown of the vertical symmetry, where the top boundary layer is thicker than the bottom one. The comparison of results against simulations performed at constant properties allows the authors to conclude that the scaling of Nu with Ra is only slightly affected by non-Oberbeck-Boussinesq conditions. [13] present measurements of the azimuthal diffusivity of large-scale circulation for Rayleigh-Bénard in a cylindrical geometry and report that what observed in the experiments [11] is indeed a transition to the "ultimate state". In the very recent work by Weiss et al. [14], the theory by Gray and Giorgini [3] is used to calculate the maximum achievable Rayleigh number within the Oberbeck–Boussinesq approximation for water, air, helium, pressurized SF6 as well as cryogenic helium. In addition [14] perform DNS of cryogenic helium and pressurized SF6 at higher Rayleigh number than the limit suggest by the theory [3]. The result is that while the most sensitive deviation from the Oberbeck-Boussinesq model is in the dependence of c_p from temperature, c_p variations do not alter significantly heat transfer characteristics. The authors conclude that the increase of γ observed in $\mathrm{Nu}\sim\mathrm{Ra}^{\gamma}$ [11], is in good part because of transition to the ultimate regime [15].

This paper focuses on Rayleigh-Bénard convection in air and evaluates typical errors in local statistics and global quantities which are to be ascribed to non-Oberbeck-Boussinesq effects. The starting point of the analysis is the work by Gray and Giorgini [3]. Results are reported from three simulations: one uses the Oberbeck–Boussinesq approximation at $\mathrm{Ra}=0.7\times10^6$ and $\mathrm{Pr}=0.7$, the other two employ the fully incompressible model at the same Rayleigh and Prandtl numbers but use reference states ($\tilde{P}_0$ and $\tilde{\Theta}_0$) and experimental parameters ($\tilde{H}$ and $\Delta\tilde{\Theta}$) because these entail different levels of non-Oberbeck-Boussinesq effects. The levels of non-Oberbeck-Boussinesq effects are graded by the relative magnitude of residuals σ, which is defined through an extension to the theory by Gray and Giorgini [3]. There, a term is deemed negligible when its magnitude is less or equal to one tenth of the non-negligible terms used for comparison. Here the idea is generalized and we use a ratio σ between the terms neglected and the terms used for comparison: $\sigma=0.1$ and $\sigma=0.05$. The accuracy in the determination of global quantities and local statistics is finally set in relation with the two selected levels of σ.

2. The governing equations of thermal convection

2.1. General framework

The governing equations for a Newtonian fluid of variable properties read

$$\begin{cases}\dfrac{\partial\tilde{\rho}}{\partial\tilde{t}}+\dfrac{\partial\tilde{\rho}\tilde{u}_j}{\partial\tilde{x}_j}=0\\ \dfrac{\partial\tilde{\rho}\tilde{u}_j}{\partial\tilde{t}}+\dfrac{\partial\tilde{\rho}\tilde{u}_i\tilde{u}_j}{\partial\tilde{x}_j}=-\dfrac{\partial\tilde{p}}{\partial\tilde{x}_i}+\dfrac{\partial\tilde{\tau}_{ij}}{\partial\tilde{x}_j}+\tilde{\rho}\tilde{g}_i\\ \tilde{\rho}\tilde{c}_p\dfrac{\partial\tilde{\Theta}}{\partial\tilde{t}}+\tilde{\rho}\tilde{c}_p\tilde{u}_j\dfrac{\partial\tilde{\Theta}}{\partial\tilde{x}_j}=\tilde{\alpha}\tilde{\Theta}\left(\dfrac{\partial\tilde{p}}{\partial\tilde{t}}+\tilde{u}_j\dfrac{\partial\tilde{p}}{\partial\tilde{x}_j}\right)+\dfrac{\partial\tilde{q}_j}{\partial\tilde{x}_j}+\tilde{\tau}_{ij}\tilde{S}_{ij}\\ \tilde{p}=f_{eq.state}\left(\tilde{\Theta},\tilde{\rho}\right)\\ \tilde{\mu}=f_{\mu}\left(\tilde{\Theta},\tilde{p}\right)\\ \tilde{\lambda}=f_{\lambda}\left(\tilde{\Theta},\tilde{p}\right)\\ \tilde{c}_p=f_{c_p}\left(\tilde{\Theta},\tilde{p}\right)\end{cases}\tag{1}$$

where the tilde $\tilde{\cdot}$ indicates dimensional quantities,

$$\tilde{\tau}_{ij}=2\tilde{\mu}\left(\tilde{S}_{ij}-\frac{1}{3}\tilde{S}_{kk}\,\delta_{ij}\right)\qquad\tilde{q}_i=\tilde{\lambda}\frac{\partial\tilde{\Theta}}{\partial\tilde{x}_i}$$

are the diffusive momentum and heat fluxes, $\tilde{\mu}$ and $\tilde{\lambda}$ are the dynamic viscosity and the thermal conductivity and

$$\tilde{S}_{ij}=\frac{1}{2}\left(\frac{\partial\tilde{u}_i}{\partial\tilde{x}_j}+\frac{\partial\tilde{u}_j}{\partial\tilde{x}_i}\right)$$

is the rate of deformation tensor. Here, $\tilde{u}_i$, $\tilde{p}$ and $\tilde{\Theta}$ are the fluid velocity, pressure and temperature, $\tilde{\rho}$ and $\tilde{c}_p$ are its density and isobaric specific heat coefficient while $\tilde{\alpha}$ is the thermal expansion coefficient. In the above equations, it is implicitly assumed that the effect of volume viscosity is negligible, i.e. the intensity of the phenomena of compression/expansion are assumed to be small enough to allow the thermodynamic property of the fluid to restore almost immediately equilibrium. In order to close the system of equations, an equation of state and thermodynamic relations for the determination of the fluid properties must be specified. In Eqs. (1), the latter are specified for the dynamic viscosity, for the thermal conductivity and for the specific heat coefficient.

A widely used model of Eqs. (1) is the Oberbeck–Boussinesq approximation [16]. It consists in assuming that all the fluid properties are constant except for density when used in the determination of buoyant forces. Furthermore, it is assumed that viscous dissipation and

the variations of internal energy with pressure are negligible. The accuracy of the approximation is addressed in the following section Section 3. The Oberbeck–Boussinesq system of equations significantly simplifies and reads

$$\begin{cases} \dfrac{\partial \tilde{u}_i}{\partial \tilde{x}_i} = 0 \\ \dfrac{\partial \tilde{u}_i}{\partial \tilde{t}} + \dfrac{\partial \tilde{u}_i \tilde{u}_j}{\partial \tilde{x}_j} = -\dfrac{1}{\tilde{\rho}_0}\dfrac{\partial \tilde{p}^*}{\partial \tilde{x}_i} + \tilde{\nu}_0 \dfrac{\partial^2 \tilde{u}_i}{\partial \tilde{x}_j \partial \tilde{x}_j} - \tilde{\alpha}_0 \tilde{g}_i \tilde{\theta} \\ \dfrac{\partial \tilde{\theta}}{\partial \tilde{t}} + \dfrac{\partial \tilde{\theta} \tilde{u}_j}{\partial \tilde{x}_j} = \tilde{\kappa}_0 \dfrac{\partial^2 \tilde{\theta}}{\partial \tilde{x}_j \partial \tilde{x}_j} \end{cases} \tag{2}$$

where it is also assumed that density variations in the buoyancy term have a linear dependence on temperature

$$\tilde{\rho} = \tilde{\rho}_0 \left(1 - \tilde{\alpha}_0 \, \tilde{\theta}\right)$$

with

$$\tilde{\theta} = \tilde{\Theta} - \tilde{\Theta}_0$$

the temperature variations. Here $\tilde{\nu} = \tilde{\mu}/\tilde{\rho}$ and $\tilde{\kappa} = \tilde{\lambda}/\tilde{\rho}\tilde{c_p}$ are the kinematic viscosity and temperature diffusivity of the fluid and the subscript 0 denotes fluid properties at a reference state. A modified pressure is also introduced, incorporating the hydrostatic potential at the reference density into the pressure gradient:

$$\tilde{p}^* = \tilde{p} + \tilde{\rho}_0 \tilde{g}_j \tilde{x}_j$$

2.2. Non-dimensional formulation

In order to have a better insight on the main features of both system of Eqs. (1) and (2), it is relevant to introduce reference scales for their non-dimensionalization. By considering the particular problem of natural convection across a flow layer where a temperature difference is imposed, the problem can be made non-dimensional by using the flow layer thickness $\tilde{H}$, the imposed temperature difference $\Delta\tilde{\Theta}$ and the free-fall velocity

$$\tilde{U}_f = \sqrt{\tilde{g}\,\tilde{\alpha}_0\,\Delta\tilde{\Theta}\,\tilde{H}}$$

that is commonly considered as a meaningful measure of the intensity of the buoyancy-driven motions. Here, $\tilde{g}$ is the magnitude of the gravity acceleration. In the case of variable fluid properties, reference values for density, dynamic viscosity, thermal conductivity and specific heat coefficient, $\tilde{\rho}_0$, $\tilde{\mu}_0$, $\tilde{\lambda}_0$ and $\tilde{c}_{p_0}$ must also be used. Accordingly, the fully compressible and variable property system of Eqs. (1) in a non-dimensional form reads

$$\begin{cases} \dfrac{\partial \rho}{\partial t} + \dfrac{\partial \rho u_j}{\partial x_j} = 0 \\ \dfrac{\partial \rho u_j}{\partial t} + \dfrac{\partial \rho u_i u_j}{\partial x_j} = -\dfrac{\partial p}{\partial x_i} + \dfrac{\sqrt{\mathrm{Pr}}}{\sqrt{\mathrm{Ra}}}\dfrac{\partial \tau_{ij}}{\partial x_j} + \dfrac{1}{\mathrm{Fr}}\rho \hat{g}_i \\ \rho c_p \dfrac{\partial \Theta}{\partial t} + \rho c_p \dfrac{\partial \Theta u_j}{\partial x_j} = \\ \qquad E\left(\dfrac{\partial p}{\partial t} + u_j \dfrac{\partial p}{\partial x_j}\right) + \dfrac{1}{\sqrt{\mathrm{Ra}\,\mathrm{Pr}}}\dfrac{\partial q_j}{\partial x_j} + \dfrac{E\sqrt{\mathrm{Pr}}}{\sqrt{\mathrm{Ra}}}\tau_{ij} S_{ij} \\ p = f_{eq.state}\left(\tilde{\Theta}, \tilde{\rho}\right)\left(\tilde{\rho}_0 \tilde{U}_f^2\right)^{-1} \\ \mu = f_\mu\left(\tilde{\Theta}, \tilde{p}\right)\tilde{\mu}_0^{-1} \\ \lambda = f_\lambda\left(\tilde{\Theta}, \tilde{p}\right)\tilde{\lambda}_0^{-1} \\ c_p = f_{c_p}\left(\tilde{\Theta}, \tilde{p}\right)\tilde{c}_{p_0}^{-1} \end{cases} \tag{3}$$

where $\hat{g}_i = \tilde{g}_i/\tilde{g}$ is the unit gravity vector. In accordance with the non-dimensional form of the governing equations, the flow solution in natural convection is determined by the Rayleigh, Prandtl, Froude and Eckert non-dimensional groups

$$\begin{aligned} \mathrm{Ra} &= \left(\frac{\tilde{U}_f\,\tilde{H}}{\tilde{\nu}_0}\right)^2 \mathrm{Pr} \\ \mathrm{Pr} &= \frac{\tilde{\nu}_0}{\tilde{\kappa}_0} \\ \mathrm{Fr} &= \frac{\tilde{U}_f^2}{\tilde{g}\,\tilde{H}} \\ E &= \frac{\tilde{U}_f^2}{\tilde{c}_{p_0}\,\Delta\tilde{\Theta}} \end{aligned} \tag{4}$$

While the Prandtl number is given by the property of the fluid in the reference state, the Rayleigh, Froude and Eckert numbers indicate the dominant processes in the flow. In particular, the Rayleigh and Froude numbers can be interpreted as a measure of the intensity of the buoyancy-driven inertial motions with respect to viscous diffusion and gravity forces, respectively while the Eckert number can be understood as a measure of the kinetic energy with respect to thermal energy. These non-dimensional groups do not uniquely determine the solution in the variable property case. Indeed, the equation of state and the constitutive relations embedded in the flow system (3) introduce a dependence of the non-dimensional flow solution also to the reference state of the flow system $(\tilde{\Theta}_0, \tilde{P}_0)$ as better shown in the next section Section 3.

This dependence on the reference state of the flow system is lost when considering the Oberbeck–Boussinesq assumption. Indeed, the non-dimensional form of the system of equations under the Oberbeck–Boussinesq assumption (1) reads

$$\begin{cases} \dfrac{\partial u_j}{\partial x_j} = 0 \\ \dfrac{\partial u_j}{\partial t} + \dfrac{\partial u_i u_j}{\partial x_j} = -\dfrac{\partial p^*}{\partial x_i} + \dfrac{\sqrt{\mathrm{Pr}}}{\sqrt{\mathrm{Ra}}}\dfrac{\partial^2 u_i}{\partial x_j \partial x_j} - \theta \hat{g}_i \\ \dfrac{\partial \theta}{\partial t} + \dfrac{\partial \theta u_j}{\partial x_j} = \dfrac{1}{\sqrt{\mathrm{Ra}\,\mathrm{Pr}}}\dfrac{\partial^2 \theta}{\partial x_j \partial x_j} \end{cases} \tag{5}$$

where the dependence of the Oberbeck–Boussinesq solution on the sole values of the Rayleigh and Prandtl numbers is now evident. By comparing the system of Eqs. (3) and (5), it is evident that low values of the Eckert number are required to make the Oberbeck–Boussinesq assumption valid. In closing this section, let us notice that it is usual to characterize natural convection in terms of the Rayleigh number rather than the widely used Grashof number,

$$\mathrm{Gr} = \frac{\mathrm{Ra}}{\mathrm{Pr}}$$

being the onset of motion from the pure conduction regime determined by a critical value of Ra.

3. Oberbeck–Boussinesq assumption: explicit conditions and validity regions

The Oberbeck–Boussinesq equations have been used over the years by almost all numerical and theoretical studies of natural convection. It is then important to address the conditions under which the Oberbeck–Boussinesq approximation can be reasonably considered as valid. A formally precise formulation that allows us to define explicit conditions that limit the applicability of the Oberbeck–Boussinesq equations has been provided by Gray and Giorgini [3]. We briefly summarize the key points in the following.

The method is based on a linearized Taylor expansion of the properties of a Newtonian fluid as a functions of two thermodynamic variables, temperature and pressure $(\tilde{\Theta}_0, \tilde{P}_0)$. By inserting these expansions on the system of governing equations and by making them

non-dimensional, different non-dimensional constant multipliers appear, providing a measure of the relative importance of the different terms of the equations. The multipliers are defined as follows,

$$\begin{aligned}
\epsilon_1 &= -\frac{1}{\tilde{\rho}_0}\left.\frac{\partial\tilde{\rho}}{\partial\tilde{\Theta}}\right|_0 \Delta\tilde{\Theta} \qquad \epsilon_2 = \frac{1}{\tilde{\rho}_0}\left.\frac{\partial\tilde{\rho}}{\partial\tilde{P}}\right|_0 \tilde{\rho}_0\tilde{g}\tilde{H} \\
\epsilon_3 &= \frac{1}{\tilde{c}_{p_0}}\left.\frac{\partial\tilde{c}_p}{\partial\tilde{\Theta}}\right|_0 \Delta\tilde{\Theta} \qquad \epsilon_4 = \frac{1}{\tilde{c}_{p_0}}\left.\frac{\partial\tilde{c}_p}{\partial\tilde{P}}\right|_0 \tilde{\rho}_0\tilde{g}\tilde{H} \\
\epsilon_5 &= \frac{1}{\tilde{\mu}_0}\left.\frac{\partial\tilde{\mu}}{\partial\tilde{\Theta}}\right|_0 \Delta\tilde{\Theta} \qquad \epsilon_6 = \frac{1}{\tilde{\mu}_0}\left.\frac{\partial\tilde{\mu}}{\partial\tilde{P}}\right|_0 \tilde{\rho}_0\tilde{g}\tilde{H} \\
\epsilon_7 &= \frac{1}{\tilde{\lambda}_0}\left.\frac{\partial\tilde{\lambda}}{\partial\tilde{\Theta}}\right|_0 \Delta\tilde{\Theta} \qquad \epsilon_8 = \frac{1}{\tilde{\lambda}_0}\left.\frac{\partial\tilde{\lambda}}{\partial\tilde{P}}\right|_0 \tilde{\rho}_0\tilde{g}\tilde{H} \\
\epsilon_9 &= \frac{1}{\tilde{\alpha}_0}\left.\frac{\partial\tilde{\alpha}}{\partial\tilde{\Theta}}\right|_0 \Delta\tilde{\Theta} \qquad \epsilon_{10} = \frac{1}{\tilde{\alpha}_0}\left.\frac{\partial\tilde{\alpha}}{\partial\tilde{P}}\right|_0 \tilde{\rho}_0\tilde{g}\tilde{H}
\end{aligned} \tag{6}$$

thus highlighting that for a given reference state $(\tilde{\Theta}_0, \tilde{P}_0)$ denoted by the subscript 0, these multipliers depend only on the working flow conditions $(\Delta\tilde{\Theta}, \tilde{H})$. The validity of the Oberbeck–Boussinesq equations requires that the multipliers of the non Oberbeck–Boussinesq terms are small,

$$|\epsilon_i| \leq \sigma \qquad i = 1, 10 \tag{7}$$

and that the multipliers to the pressure work and viscous dissipation terms in the thermal energy equation are also small,

$$\begin{aligned}
&\left|\frac{\tilde{\alpha}_0}{\tilde{c}_{p_0}}\left(\frac{\tilde{g}\tilde{H}\tilde{\Theta}_0}{\Delta\tilde{\Theta}}\right)\right| \leq \sigma \\
&\left|\frac{\tilde{\alpha}_0}{\tilde{c}_{p_0}}\left(\tilde{g}\tilde{H}\right)\right| \mathrm{Pr} \leq \sigma
\end{aligned} \tag{8}$$

where $\sigma \ll 1$ is a threshold identifying an acceptable deviation from the strict Boussinesq behavior. For the complete derivation of Eqs. (6) and (8) the reader is referred to Gray and Giorgini [3]. Eqs. (7) and (8) can be recast as

$$\begin{aligned}
\Delta\tilde{\Theta} &\leq \sigma\left|\frac{1}{\tilde{\rho}}\left.\frac{\partial\tilde{\rho}}{\partial\tilde{\Theta}}\right|_0\right|^{-1} \qquad \tilde{H} \leq \sigma\left|\tilde{g}\left.\frac{\partial\tilde{\rho}}{\partial\tilde{P}}\right|_0\right|^{-1} \\
\Delta\tilde{\Theta} &\leq \sigma\left|\frac{1}{\tilde{c}_p}\left.\frac{\partial\tilde{c}_p}{\partial\tilde{\Theta}}\right|_0\right|^{-1} \qquad \tilde{H} \leq \sigma\left|\frac{\tilde{\rho}\tilde{g}}{\tilde{c}_p}\left.\frac{\partial\tilde{c}_p}{\partial\tilde{P}}\right|_0\right|^{-1} \\
\Delta\tilde{\Theta} &\leq \sigma\left|\frac{1}{\tilde{\mu}}\left.\frac{\partial\tilde{\mu}}{\partial\tilde{\Theta}}\right|_0\right|^{-1} \qquad \tilde{H} \leq \sigma\left|\frac{\tilde{\rho}\tilde{g}}{\tilde{\mu}}\left.\frac{\partial\tilde{\mu}}{\partial\tilde{P}}\right|_0\right|^{-1} \\
\Delta\tilde{\Theta} &\leq \sigma\left|\frac{1}{\tilde{\lambda}}\left.\frac{\partial\tilde{\lambda}}{\partial\tilde{\Theta}}\right|_0\right|^{-1} \qquad \tilde{H} \leq \sigma\left|\frac{\tilde{\rho}\tilde{g}}{\tilde{\lambda}}\left.\frac{\partial\tilde{\lambda}}{\partial\tilde{P}}\right|_0\right|^{-1} \\
\Delta\tilde{\Theta} &\leq \sigma\left|\frac{1}{\tilde{\alpha}}\left.\frac{\partial\tilde{\alpha}}{\partial\tilde{\Theta}}\right|_0\right|^{-1} \qquad \tilde{H} \leq \sigma\left|\frac{\tilde{\rho}\tilde{g}}{\tilde{\alpha}}\left.\frac{\partial\tilde{\alpha}}{\partial\tilde{P}}\right|_0\right|^{-1} \\
\frac{\tilde{H}}{\Delta\tilde{\Theta}} &\leq \sigma\left|\frac{\tilde{\alpha}\tilde{g}\tilde{\Theta}}{\tilde{c}_p}\right|_0^{-1} \qquad \tilde{H} \leq \sigma\left|\mathrm{Pr}\frac{\tilde{\alpha}\tilde{g}}{\tilde{c}_p}\right|_0^{-1}
\end{aligned} \tag{9}$$

Eqs. (9) represent a system of explicit conditions that pose limits to the working flow conditions $(\Delta\tilde{\Theta}, \tilde{H})$ for any given Newtonian fluid and reference state condition $(\tilde{\Theta}_0, \tilde{P}_0)$. Notice that these conditions are not limited to any particular geometry.

The validity region of the Oberbeck–Boussinesq approximation for natural convection problems where air is the working fluid for a reference state $(\tilde{\Theta}_0, \tilde{P}_0)$ = (30 °C, 1 atm) is reported in Fig. 1. The limits of validity have been defined by using the value σ = 0.1, i.e. a 10% tolerance on variations of thermophysical properties around reference state values is admitted [3]. The plot allows us to clearly understand the role played by each property of the fluid in limiting the applicability of the Oberbeck–Boussinesq approximation. From Fig. 1, it is immediately apparent how the limits in the working flow conditions are more compelling for the temperature difference $\Delta\tilde{\Theta}$ than for the characteristic length $\tilde{H}$, see also Table 1 where limiting values are reported for different reference state conditions. These limits on $(\Delta\tilde{\Theta}, \tilde{H})$ pose also constraints in the maximum Rayleigh number achievable under the validity of the

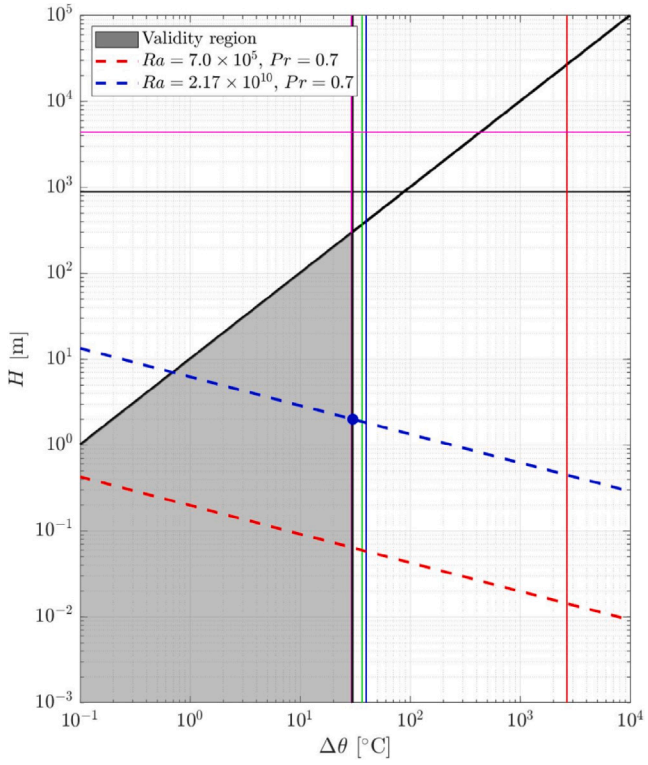

Fig. 1. Validity regions of the Oberbeck–Boussinesq equations for a $\sigma = 0.1$ tolerance, using air as working fluid, for a fixed reference state $(\tilde{\Theta}_0, \tilde{P}_0)$ = (30 °C, 1 atm). Horizontal lines denote the limit of applicability of the Oberbeck–Boussinesq equations on the characteristic length scale of the problem $\tilde{H}$ given by the variation of the fluid properties with pressure (conditions in the right column of (9)). The vertical lines denote the limit of applicability of the Oberbeck–Boussinesq equations on the characteristic temperature difference of the problem $\Delta\tilde{\Theta}$ given by the variation of the fluid properties with temperature (conditions in the left column of (9)). Colors identify the fluid variable associated with the validity condition: density $\tilde{\rho}$ (black), dynamic viscosity $\tilde{\mu}$ (blue), isobaric heat coefficient $\tilde{c}_p$ (red), thermal conductivity $\tilde{\lambda}$ (green) and thermal expansion coefficient $\tilde{\alpha}$ (violet). The inclined black line denotes the limit imposed by the pressure work term being negligible (last condition in the left column of (9)). The dashed lines display values of the working flow conditions $(\Delta\tilde{\Theta}, \tilde{H})$ at constant Rayleigh number. The red dashed line corresponds to the Ra investigated in the present work, while the blue dashed line corresponds to the maximum Ra that can be experimentally investigated in a tank of air whose height is $\tilde{H} = 2m$. (For interpretation of the references to color in this figure legend, the reader is referred to the web version of this article.)

Oberbeck–Boussinesq equations, see again Table 1. All these aspects should be carefully taken into account especially when comparing numerical simulations performed using the Oberbeck–Boussinesq assumption with experiments that, as shown by the plot in Fig. 1, can easily exceed the limits of its validity. Caution must be taken also when considering experiments using water as the working fluid, as shown in Table 1. In this respect, the increase of the reference temperature $\tilde{\Theta}_0$ partially mitigate this issue by slightly expanding the validity region, see again Table 1. The range of validity of the Oberbeck–Boussinesq approximation is slightly wider in a physical system characterized by high reference temperatures.

Obviously, the constraints on the validity of the Oberbeck–Boussinesq approximation become more strict for small tolerances σ. As shown in Table 2, a significant reduction in the maximum temperature difference $\Delta\tilde{\Theta}_{max}$ and in the size of the cell $\tilde{H}_{max}$ is required to decrease the tolerance from σ = 0.15 to σ = 0.05. This also leads to a significant decrease in the maximum Rayleigh number achievable, see again Table 2.

Table 1
Limiting values of the working flow conditions $(\Delta\tilde{\Theta}_{max}, \tilde{H}_{max})$ and of the Rayleigh number achievable Ra_{max} under the validity of the Oberbeck–Boussinesq equations for $\sigma = 0.1$.

Fluid	$\tilde{\Theta}_0$	$\tilde{P}_0$	$\Delta\tilde{\Theta}_{max}$	$\tilde{H}_{max}$	Ra_{max}
Air	30 °C	1 atm	28.2 °C	269 m	4.93×10^{16}
Air	50 °C	1 atm	31.3 °C	311 m	6.12×10^{16}
Air	70 °C	1 atm	33.2 °C	343 m	6.74×10^{16}
Water	15 °C	1 atm	1.3 °C	1260 m	2.38×10^{19}
Water	30 °C	1 atm	3.5 °C	1610 m	3.65×10^{20}

Table 2
Dependence of the limiting values of the working flow conditions $(\Delta\tilde{\Theta}_{max}, \tilde{H}_{max})$ on the threshold σ for a fixed reference state $(\tilde{\Theta}_0, \tilde{P}_0) = (30\ °C, 1\ atm)$.

Fluid	σ	$\Delta\tilde{\Theta}_{max}$	$\tilde{H}_{max}$	Ra_{max}
air	0.05	14.1 °C	67 m	3.74×10^{14}
Air	0.1	28.2 °C	269 m	4.93×10^{16}
Air	0.15	42.3 °C	605 m	8.27×10^{17}
Water	0.05	1.7 °C	403 m	2.85×10^{18}
Water	0.1	3.5 °C	1610 m	3.65×10^{20}
Water	0.15	5.2 °C	3623 m	6.24×10^{21}

4. Direct numerical simulations of Rayleigh–Bénard convection

In accordance with the above reasoning, experiments in natural convection are likely to be influenced by non-Oberbeck–Boussinesq phenomena. On the contrary, numerical simulations are almost always performed by solving the Oberbeck–Boussinesq equations. This aspect represents an issue especially for research topics such as the ultimate regime of natural convection [17] where both experimental and numerical data are often used together to assess the scaling of heat transfer. The risk is that anomalous scaling can rise due to the collection of data where non-Oberbeck–Boussinesq effects are randomly included. As a consequence, the characterization of the effects of non-Oberbeck–Boussinesq phenomena on the main features of natural convection in the turbulent regime is deemed of relevant importance. Such information would help in clarifying and possibly correct anomalous scaling in data set including both numerical and experimental data and would be a further step toward a better comprehension of turbulent thermal convection.

In the present work we aim at addressing the issue of non-Oberbeck–Boussinesq effects by performing direct numerical simulations of Rayleigh–Bénard convection using both the Oberbeck–Boussinesq equations (2) and the full system of Eqs. (1) under two validity conditions $\sigma = 0.1$ and 0.05, i.e. when a 10% and 5% tolerance on variations of thermophysical properties around reference state values is admitted, respectively. The use of two values of σ allows us to assess also the actual conditions to be verified in experiments in order to avoid non-Oberbeck–Boussinesq effects.

4.1. Numerical settings

The full governing equations (1) and the Oberbeck–Boussinesq equations (2) have been solved using the finite volume solver OpenFOAM in the settings of a Rayleigh–Bénard cell at $\mathrm{Ra} = 0.7 \times 10^6$ and $\mathrm{Pr} = 0.7$. For the variable property flow case, the equation of state for a perfect gas is used together with the Sutherland's law for viscosity and the modified Eucken correlation [18] for the thermal conductivity. The JANAF tables are finally used to compute the c_p coefficient in a polynomial form, even though the dependence of the specific heat with temperature for air at the chosen reference state is practically negligible.

Second-order central schemes are used to discretize space while a second-order implicit scheme is used for time integration. The equations are solved in a numerical domain whose dimensions are $(L_x, L_y, L_z) = (8H, H, 8H)$. Here x (u), y (v) and z (w) denote the streamwise, wall-normal and spanwise directions (velocities), respectively. Periodic boundary conditions are applied in the wall-parallel directions. At the top and bottom walls constant temperature values are imposed. The domain is discretized with $(N_x, N_y, N_z) = (256, 130, 256)$ volumes. The grid elements are homogeneously distributed in the wall-parallel directions and clustered at the wall in the wall-normal directions. The resulting spatial resolution in terms of Kolmogorov length scales is $(\Delta x, \Delta y|_w, \Delta z)/\eta_w = (2.81, 0.48, 2.81)$ where η_w is the Kolmogorov scale evaluated at the wall, i.e. the smallest value reached within the flow. Further details about the grid resolution and the validation of the numerical results are reported in Appendix.

Statistics are computed by performing a spatial average along the wall-parallel directions and a temporal average over 33 flow samples gathered every $15H/U_f$ times after the initial flow transient has been washed out. The resulting average operator will be denoted with $\langle\cdot\rangle$. The Favre decomposition of variable property flow quantities in a mean and fluctuating field will be also adopted that for a generic quantity β reads

$$\beta = \langle\beta\rangle_F + \beta'' \tag{10}$$

where the Favre average is defined as $\langle\beta\rangle_F = \langle\rho\beta\rangle/\langle\rho\rangle$.

4.2. Flow configuration

As already shown in Section 2, the non-dimensional solution of the Oberbeck–Boussinesq equations (5) depends only on the values of the Rayleigh (Grashof) and Prandtl numbers. Here, we selected $\mathrm{Ra} = 0.7\times10^6$ and $\mathrm{Pr} = 0.7$. This value of the Prandtl number is independent of the working flow conditions $(\Delta\tilde{\Theta}, \tilde{H})$ and is representative of air in a wide range of reference state conditions, say $0\ °C < \tilde{\Theta}_0 < 400\ °C$ and $1\ atm < \tilde{P}_0 < 20\ atm$. On the contrary, the Rayleigh number is strongly dependent on the working flow conditions $(\Delta\tilde{\Theta}, \tilde{H})$ meaning that the non-dimensional solution of the Oberbeck–Boussinesq equations (5) is representative of all the possible combinations of $(\Delta\tilde{\Theta}, \tilde{H})$ that give the same Rayleigh number. In particular, for a given Rayleigh number Ra_0 the combination of working flow conditions is

$$\tilde{H} = \left(\frac{\tilde{\nu}_0\tilde{\kappa}_0}{\tilde{g}\tilde{\alpha}_0}\mathrm{Ra}_0\right)^{1/3} \Delta\tilde{\Theta}^{-1/3} \tag{11}$$

and is reported with a red dashed line in Fig. 1.

Contrary to the Oberbeck–Boussinesq approach, the non-dimensional solution of the full governing equations (3) depends also on the specific reference state of the flow system $(\tilde{\Theta}_0, \tilde{P}_0)$ and on the specific working flow conditions $(\Delta\tilde{\Theta}, \tilde{H})$ through the equation of state and the constitutive relations embedded in the flow system (3). Hence, the flow solution of the full governing equations (3) is representative of a single combination of working flow conditions and reference states $(\Delta\tilde{\Theta}, \tilde{H}, \tilde{\Theta}_0, \tilde{P}_0)$ for a given fluid. From a non-dimensional point of view, this specificity is highlighted by the dependence of the solution also on the Froude and Eckert numbers, beside the Rayleigh (Grashof) and Prandtl numbers. Indeed, these two additional non-dimensional groups prescribe the characteristic temperature difference and length of the problem. In particular, for a given Froude number Fr_0 a constant value of $\Delta\tilde{\Theta}$ is prescribed for each reference state condition,

$$\Delta\tilde{\Theta} = \frac{Fr_0}{\alpha_0} \tag{12}$$

On the other hand, for a given Eckert number E_0 a constant value of $\tilde{H}$ is prescribed for each reference state condition,

$$\tilde{H} = \frac{\tilde{c}_{p_0}}{\tilde{g}\tilde{\alpha}_0}E_0 \tag{13}$$

Hence, the non-dimensional solution of the full governing equations (3) is representative of a single reference state of the flow system $(\tilde{\Theta}_0, \tilde{P}_0)$ and of a single working flow condition $(\Delta\tilde{\Theta}, \tilde{H})$ corresponding to a Rayleigh number given by the intercept of relations (12) and (13), i.e.

$$\mathrm{Ra} = \frac{\tilde{c}_{p_0}}{\tilde{\alpha}_0\tilde{\kappa}_0\tilde{\nu}_0}E\,\mathrm{Fr} \tag{14}$$

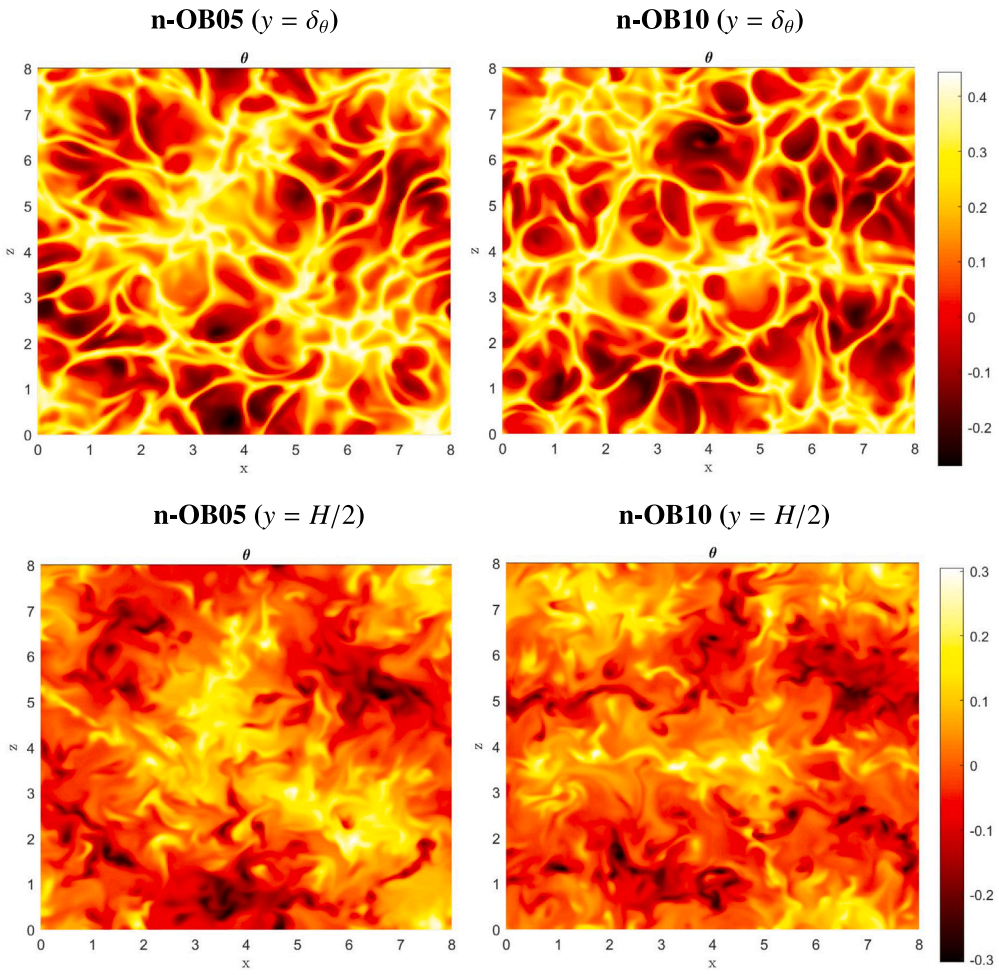

Fig. 2. Direct numerical simulations of Rayleigh–Bénard convection at $\mathrm{Ra} = 0.7 \times 10^6$ and $\mathrm{Pr} = 0.7$: instantaneous temperature fields n-OB05 case (left panels) and for the n-OB10 case (right panels) evaluated at the edge of the thermal boundary layer $y = \delta_\theta$ (top panels) and at the cell mid plane $y = H/2$ (bottom panels).

In accordance with the above reasoning, the full system of variable property equations (1) has been solved for a specific reference state $(\tilde{\Theta}_0, \tilde{P}_0) = (30\ ^\circ\mathrm{C},\ 1\ \mathrm{atm})$ with air as working fluid, i.e. $\mathrm{Pr} = 0.7$. Two different working flow conditions have been selected both giving $\mathrm{Ra} = 0.7{\times}10^6$. The first one, $(\Delta\tilde{\Theta}, \tilde{H}) = (30\ ^\circ\mathrm{C}, 0.064\ \mathrm{m})$, has been chosen in order to study non-Oberbeck–Boussinesq effects in flow conditions where $\sigma = 0.1$, i.e. when the Oberbeck–Boussinesq assumptions are considered valid within a 10% of tolerance. These values correspond to $\mathrm{Fr} = 1.006$ and $E = 2.07 \times 10^{-6}$. The second working flow condition selected is $(\Delta\tilde{\Theta}, \tilde{H}) = (15\ ^\circ\mathrm{C}, 0.08\ \mathrm{m})$, corresponds to $\sigma = 0.05$ and has been selected in order to investigate reliable values of σ for the recovery of the Oberbeck–Boussinesq flow solutions. These values correspond to $\mathrm{Fr} = 0.957$ and $E = 2.59 \times 10^{-6}$. Let us notice that, in both flow cases, the threshold values in the variation of the thermophysical properties of the fluid σ are given by the conditions for ϵ_1 and ϵ_9. A view of the instantaneous pattern taken by the temperature field at the edge of the thermal boundary layer and at the cell half-height is reported in Fig. 2 for both simulations.

The very small values taken by the Eckert number in both the flow conditions examined, suggests that the Oberbeck–Boussinesq assumption of a negligible role played by the viscous dissipation and pressure work in the energy balance is actually reasonable. As expected, the Eckert number assumes a smaller valuer for the $\sigma = 0.1$ case thus suggesting that thermal energy covers a more important role in the determination of the flow solution than in the $\sigma = 0.05$ case.

For the sake of brevity, the flow solution of the Oberbeck–Boussinesq equations (2) will be referred to as the OB case. On the other hand, the flow solution of the variable property equations (1) at flow conditions corresponding to a 10% of tolerance of validity of the Oberbeck–Boussinesq assumption ($\sigma = 0.1$) will be denoted to as n-OB10 while that corresponding to a 5% of tolerance as n-OB05.

5. Non-Oberbeck–Boussinesq effects under different validity conditions

We start the analysis by considering first the behavior of the Nusselt number when non-Oberbeck–Boussinesq effects are taken into account for two different validity conditions, $\sigma = 0.05$ and 0.1. We measure $Nu = 7.38$, 7.22 and 8.16 for the OB, n-OB05 and n-OB10 cases respectively. It is then evident that the non-Oberbeck–Boussinesq effects are relevant also for integral quantities such as the overall heat transfer rate of the flow system. Notice that this quantity measured by the Nusselt number is of primary interest for both research and applications. The present results unequivocally show from a quantitative point of view that non-Oberbeck–Boussinesq effects can be neglected only for flow conditions $(\Delta\tilde{\Theta}, \tilde{H})$ that allow for a maximum of a 5% on variations of the thermophysical properties around reference state values ($\sigma = 0.05$). This conclusion applies also for almost all the statistical feature of the flow as shown in the following.

In Fig. 3, the mean temperature profiles for the three simulated flow cases are reported. The solution of the Oberbeck–Boussinesq system of Eqs. (2) is found to collapse with the solution of the full variable property equations (1) when a tolerance $\sigma = 0.05$ is admitted. On the contrary, when $\sigma = 0.1$ a significant deviation in the temperature

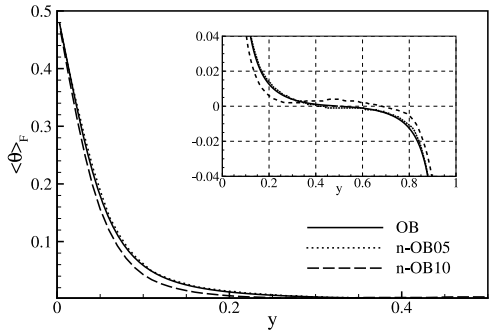

Fig. 3. Rayleigh–Bénard convection at Ra = 0.7×10^6 and Pr = 0.7: mean temperature profiles for the OB case (solid), for the n-OB05 case (dotted) and for the n-OB10 case (dashed). The inset plot shows an enlarged view of the temperature profiles in the core of the flow.

profiles is observed as well as a loss of up-down symmetry in the mean solution [19], see also the inset plot in Fig. 3. In particular, a steeper decrease of temperature profile is induced by non-Oberbeck–Boussinesq effects when $\sigma = 0.1$ is admitted, in accordance with the previously observed increase of the overall amount of heat transfer measured by Nu. This increase of mixing is not accompanied by an increase of the intensity of the temperature fluctuations. On the contrary, the temperature variance is found to actually decrease when non-Oberbeck–Boussinesq effects with tolerance $\sigma = 0.1$ are considered, see Fig. 4(a). This decrease in the intensity of the temperature fluctuations reflects on the intensity of the velocity fluctuations induced through buoyancy. As shown in Fig. 4(b), the variance of both the wall-normal and wall-parallel velocity fluctuations indeed decrease when non-Oberbeck–Boussinesq effects with tolerance $\sigma = 0.1$ are considered, in line with the observed reduction of the temperature fluctuations. Again, when a flow case with a 5% tolerance on variations of the thermophysical properties is considered, the non-Oberbeck–Boussinesq effects are found to be almost negligible also for the turbulent intensities. As shown in Fig. 4(a) and (b), the variance of both temperature and velocity fluctuations is indeed found to recover the behavior of the Oberbeck–Boussinesq solution when $\sigma = 0.05$.

It is worth now trying to investigate the origin of the increase of mixing induced by non-Oberbeck–Boussinesq effects with tolerance $\sigma = 0.1$. In accordance with the previous analysis, the increase in the Nusselt number is not induced by an increase of the intensity of the temperature and velocity fluctuations, see again Fig. 4(a) and (b). A possible explanation of this increase can be than given by the analysis of the third- and fourth-order statistical moments of the temperature field. In Fig. 5, the skewness S_θ and kurtosis K_θ of the temperature field are reported. Non-Oberbeck–Boussinesq effects are again found to be negligible when a 5% tolerance is considered ($\sigma = 0.05$). On the contrary, for the flow conditions corresponding to a 10% tolerance on the variations of the fluid properties ($\sigma = 0.1$), an increase of both the skewness and kurtosis is observed. A possible interpretation is the following.

The skewness of temperature fluctuations in Rayleigh–Bénard convection is generally negative near the wall and positive away from it, see again Fig. 5(a). The change of sign occurs at the thermal boundary layer thickness evaluated as $\delta_\theta = H/2Nu$ that in the present flow cases is $\delta_\theta = 0.07$ for the OB and n-OB05 cases while $\delta_\theta = 0.06$ for the n-OB10 case. The negative sign of the skewness highlights the presence of small areas of intense negative fluctuations of temperature within the thermal boundary layer. On the contrary, the positive sign of the skewness unveils the presence of small areas of intense positive fluctuations of temperature in the bulk of the flow. Notice that skewness has an odd behavior with respect to the cell center. Accordingly, the thermal boundary layers are characterized by extreme events of wall impingement of plumes while the bulk of the flow by extreme events

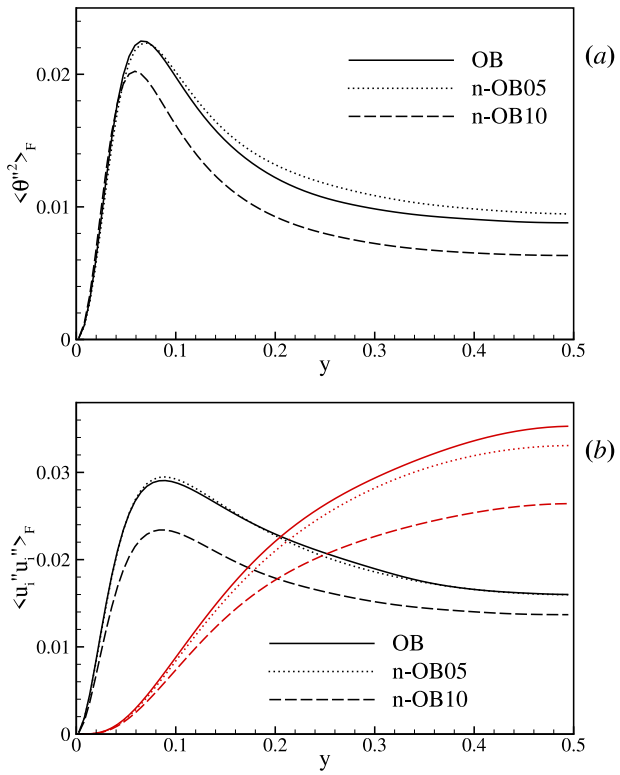

Fig. 4. Rayleigh–Bénard convection at Ra = 0.7×10^6 and Pr = 0.7. (a) Temperature variance profiles and (b) vertical (red) and wall-parallel (black) velocity variance profiles for the OB case (solid), for the n-OB05 case (dotted) and for the n-OB10 case (dashed).

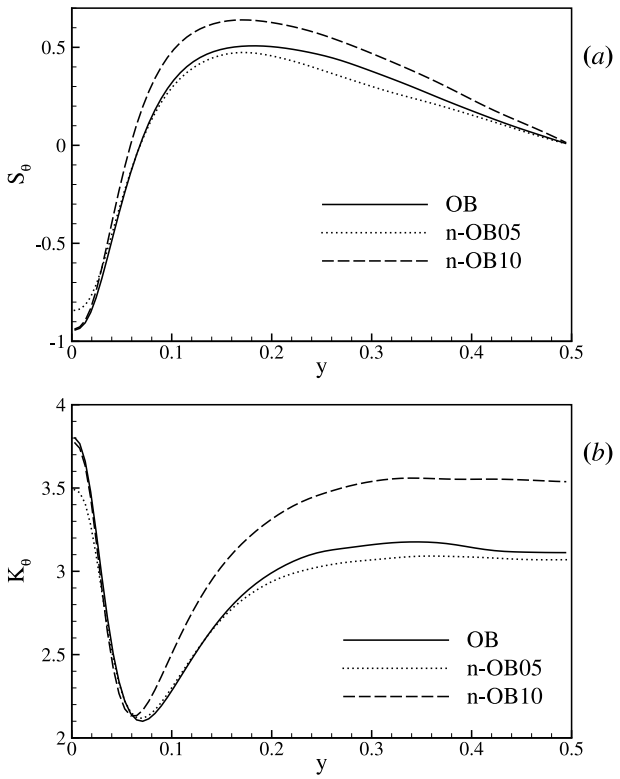

Fig. 5. Rayleigh–Bénard convection at Ra = 0.7×10^6 and Pr = 0.7. (a) Third-order moment S_θ and (b) fourth-order moment K_θ of temperature profiles for the OB case (solid), for the n-OB05 case (dotted) and for the n-OB10 case (dashed).

Table 3
Limiting values of the maximum temperature difference $\Delta\tilde{\Theta}_{max}$ that can be imposed in a $\tilde{H} = 2$ m tank experiment and of the Rayleigh number achievable Ra_{max} under the validity of the Oberbeck–Boussinesq equations for $\sigma = 0.05$.

Fluid	$\tilde{\Theta}_0$	$\tilde{P}_0$	$\Delta\tilde{\Theta}_{max}$	$\tilde{H}$	Ra_{max}
Air	30 °C	1 atm	14.1 °C	2 m	0.99×10^{10}
Air	50 °C	1 atm	15.6 °C	2 m	0.82×10^{10}
Air	70 °C	1 atm	16.6 °C	2 m	0.67×10^{10}
Water	15 °C	1 atm	0.6 °C	2 m	4.76×10^{10}
Water	30 °C	1 atm	1.7 °C	2 m	3.50×10^{11}

of plumes ejected from the walls and traversing the cell height. The fact that skewness in the bulk is more intense in flow conditions where a 10% tolerance on the variations of the fluid properties occurs ($\sigma = 0.1$) suggests that non-Oberbeck–Boussinesq effects manifest in plume ejection events carrying an higher temperature difference with respect to the background. The observed increase of kurtosis at values higher than the classical Gaussian distribution, further suggests that non-Oberbeck–Boussinesq mechanisms make the bulk of the flow more and more dominated by these intermittent and extreme events. Accordingly, we might conjecture that the increase of mixing induced by non-Oberbeck–Boussinesq phenomena and measured with Nu is related with the establishment of a flow pattern of thinner but more intense thermal plumes traversing the cell height, see the instantaneous pattern taken by the temperature field at the cell mid-plane reported in the bottom panels of Fig. 2. This pattern is more efficient in carrying out heat exchange between the two walls even if is associated with a smaller temperature variance due to the relative small area occupied by such plume structures.

6. Final remarks

Results from three direct numerical simulations are presented to assess non-Oberbeck–Boussinesq effects on Rayleigh–Bénard convection of air at $\mathrm{Ra} = 0.7 \times 10^6$ and $\mathrm{Pr} = 0.7$. One DNS, identified in the text by the acronym OB, numerically solves the incompressible system of equations derived from the Oberbeck–Boussinesq assumption. In this case the solution is fully determined by the Rayleigh and Prandtl numbers. The other two simulations (n-OB05 and n-OB10) employ a variable-density formulation, include viscous dissipation and pressure work in the energy equation and account for the dependency of fluid properties ($\tilde{\rho}$, $\tilde{\mu}$, $\tilde{\lambda}$ and $\tilde{c}_p$) on pressure and temperature. In this case, the non-dimensional solution depends additionally on the Froude and Eckert numbers, on the fluid (through the state equations used), on experimental conditions ($\Delta\tilde{\Theta}, \tilde{H}$) and reference states ($\tilde{\Theta}_0, \tilde{P}_0$). By using the formalism provided by Gray and Giorgini [3], simulations n-OB05 and n-OB10 are designed to share the same Rayleigh and Prandtl numbers of the incompressible solution but for two different levels of tolerance on variations of the thermophysical properties of the fluid: $\sigma = 0.05$ and $\sigma = 0.1$, respectively. This is obtained by tuning the experimental conditions $(\Delta\tilde{\Theta}, \tilde{H}) = (30\ °\mathrm{C}, 0.064\ \mathrm{m})$ and $(\Delta\tilde{\Theta}, \tilde{H}) = (15\ °\mathrm{C}, 0.08\ \mathrm{m})$ for the two n-OB cases, while keeping the same reference state $(\tilde{\Theta}_0, \tilde{P}_0) = (30°)$ C, 1 atm).

The statistical analysis of the simulations reveals that using air as the working fluid and for the experimental conditions selected, non-Oberbeck–Boussinesq phenomena significantly affect local and global results when a 10% tolerance ($\sigma = 0.1$) is allowed. The non-Oberbeck–Boussinesq effects consist in a decrease in the intensity of turbulent fluctuations of temperature and velocity and an increased mixing. Accordingly, a non-negligible heat transfer enhancement is observed in the variable property solution: it consists in a 10% Nusselt number increase ($Nu = 7.38$ for the OB case and $Nu = 8.16$ for then-OB10 case). Instead, when a 5% tolerance on the variations of the thermophysical properties is considered ($\sigma = 0.05$), the non-Oberbeck–Boussinesq effects are found to be negligible in both the global and local statistics.

Although there have been several significant works devoted to understanding and quantifying non-Oberbeck–Boussinesq effects, the present results demonstrate how suitable the use of DNS data combined with the Gray and Giorgini's theoretical framework is for the design of numerical and experimental campaigns for the study of Rayleigh–Bénard convection. As an example, by considering an experiment of turbulent Rayleigh–Bénard convection performed in a tank of height $\tilde{H} = 2$ m filled with air at $\tilde{P}_0 = 1$ atm, the maximum Rayleigh number that can be investigated without the influence of non-Oberbeck–Boussinesq phenomena is rather low of the order of 10^{10}, see Table 3 and the blue dashed line in Fig. 1. In the hypothesis that also for water the Oberbeck–Boussinesq approximation is acceptable for $\sigma = 0.05$, the maximum Rayleigh number that can be investigated without the influence of non-Oberbeck–Boussinesq phenomena with water as working fluid is also rather low of the order of 10^{11}, see again Table 3. By further considering that these limiting values of Rayleigh number cubically decrease with decreasing tank heights, it is reasonable to conclude that experiments are almost always affected by non-Oberbeck–Boussinesq phenomena. These phenomena are quantitatively shown here to modify also integral properties such as the Nusselt number. Hence, gathering results from experiments with those from numerical simulations can easily lead to incorrect interpretations when the latter are performed under the Oberbeck–Boussinesq assumption. In conclusion, the present results clearly support the use of DNS data combined with the Gray and Giorgini's theoretical framework as a best practice for the design of research activities involving both numerical and experimental data.

CRediT authorship contribution statement

A. Cimarelli: Writing – review & editing, Writing – original draft, Supervision, Project administration, Formal analysis, Conceptualization. **A. Fenzi:** Investigation, Data curation. **D. Angeli:** Supervision, Software, Data curation. **E. Stalio:** Writing – original draft, Supervision.

Declaration of competing interest

The authors declare that they have no known competing financial interests or personal relationships that could have appeared to influence the work reported in this paper.

Acknowledgments

The authors acknowledge PRACE for awarding access to the Marconi-KNL cluster (CINECA, Italy) through Call 17.

Project funded under the National Recovery and Resilience Plan (NRRP), Mission 4 Component 2 Investment 1.5-Call for Tender No. 3277 of 30/12/2021 of the Italian Ministry of University and Research funded by the European Union—NextGenerationEU. Award Number: Project code ECS00000033, Concession Decree No. 1052 of 23/06/2022 adopted by the Italian Ministry of University and Research, CUP E95F21003430001, "Ecosystem for Sustainable Transition in Emilia-Romagna" (Ecosister).

Appendix. Assessment of the spatial resolution and validation

The present simulations of Rayleigh–Bénard convection at $\mathrm{Ra} = 0.7 \times 10^6$ and $\mathrm{Pr} = 0.7$ have been performed using a finite volume second-order accurate discretization in a structured Cartesian grid. The domain size is $(8H, H, 8H)$ and the number of volumes used is $(256, 130, 256)$ that are homogeneously distributed in the two horizontal directions and stretched in the vertical one in order to achieve higher levels of resolution in the near-wall region. As already stated in the main body of the work, the corresponding resolution at the wall where the Kolmogorov scale reaches its minimum value is $(\Delta x, \Delta y|_w, \Delta z)/\eta_w = (2.81, 0.48, 2.81)$. This spatial resolution satisfies classical requirements

for a direct numerical simulation. However, in order to further validate the numerical approach used, we report here a deeper assessment of the spatial resolution of the overall numerical method and a validation of our results against the high-order spectral simulation performed by Togni et al. [20].

A critical numerical aspect to conduct accurate numerical simulations of turbulent Rayleigh–Bénard convection is the number of grid points used to discretize the thermal and kinetic boundary layers. An universal criterion to determine the adequate grid resolution within the boundary layers has been derived in [21] and for the particular case of $Pr = 0.7$ takes the following approximate form,

$$N_{BL,\theta} \approx 0.35\,\mathrm{Ra}^{0.15}$$
$$N_{BL,u} \approx 0.31\,\mathrm{Ra}^{0.15} \tag{A.1}$$

where $N_{BL,\theta}$ and $N_{BL,u}$ indicate the prescribed minimum number of grid points inside the thermal and kinetic boundary layers, respectively. For the present value of the Rayleigh number, this criterion leads to $N_{BL,\theta} \approx 2.63$ and $N_{BL,u} \approx 2.33$. By evaluating the thermal and kinetic boundary layer thicknesses as

$$\delta_\theta = \frac{H}{2\mathrm{Nu}}$$
$$\delta_u = \frac{H\,\mathrm{Pr}^{(0.357-0.022\log \mathrm{Pr})}}{2\mathrm{Nu}} \tag{A.2}$$

where the latter is an exact relation provided by Shishkina et al. [21], we measure that our simulations make use of 17 and 15 grid points within them thus largely exceeding the recommended minimum requirements.

A classical way to further assess the resolution is by checking the degree to which the *consistency relations* are fulfilled by the numerical data set. These exact relations can be derived from the governing equations [22] and allow us to estimate the Nusselt number by using different statistical observables which are separately affected by the spatial resolution,

$$Nu_1 = 1 + \sqrt{\mathrm{Ra}\,\mathrm{Pr}}\langle v'\theta'\rangle_V \tag{A.3}$$
$$Nu_2 = 1 + \sqrt{\mathrm{Ra}\,\mathrm{Pr}}\langle \tilde{\epsilon}\rangle_V \tag{A.4}$$
$$Nu_3 = 1 + \sqrt{\mathrm{Ra}\,\mathrm{Pr}}\langle \tilde{\epsilon}_\theta\rangle_V \tag{A.5}$$

Here, $\langle\cdot\rangle_V$ indicates the volume average on the whole domain, while $\tilde{\epsilon}$ and $\tilde{\epsilon}_\theta$ are respectively the pseudo-dissipation rate of kinetic energy and of square temperature,

$$\langle \tilde{\epsilon}\rangle_V = \frac{\sqrt{\mathrm{Pr}}}{\sqrt{\mathrm{Ra}}}\left\langle \frac{\partial u_i}{\partial x_j}\frac{\partial u_j}{\partial x_i}\right\rangle_V \tag{A.6}$$
$$\langle \tilde{\epsilon}_\theta\rangle = \frac{1}{\sqrt{\mathrm{Ra}\,\mathrm{Pr}}}\left\langle \frac{\partial \theta}{\partial x_i}\frac{\partial \theta}{\partial x_i}\right\rangle_V \tag{A.7}$$

The use of the consistency relations with data from the OB, n-OB05 and n-OB10 cases leads to estimates of the Nusselt number that deviate by a maximum of 2% from the nominal one computed with the averaged temperature gradient at the wall.

Finally, in order to validate the overall numerical method we performed an additional direct numerical simulation under the Oberbeck–Boussinesq approximation at $\mathrm{Ra} = 1.7 \times 10^5$ and $\mathrm{Pr} = 0.7$ in order to match the parameters of the high-fidelity spectral simulation performed by Togni et al. [20]. The domain size is $(8H, H, 8H)$ and the number of volumes used is $(128, 130, 128)$. The numeric settings and the grid properties are the same used for the OB, n-OB05 and n-OB10 cases analyzed in the present work. In order to validate the integral properties of the solution, we compute first the Nusselt number. We measure $\mathrm{Nu} = 5.00$ that closely agrees with $\mathrm{Nu} = 4.98$ computed by Togni et al. [20]. On the other hand, the profiles of first- and second-order statistics, as computed with the present method and compared with the reference data are reported in Fig. A.6. The very good agreement also for these statistics and the quality of the spatial resolution tests reported so far suggest that the overall accuracy of the present results is good.

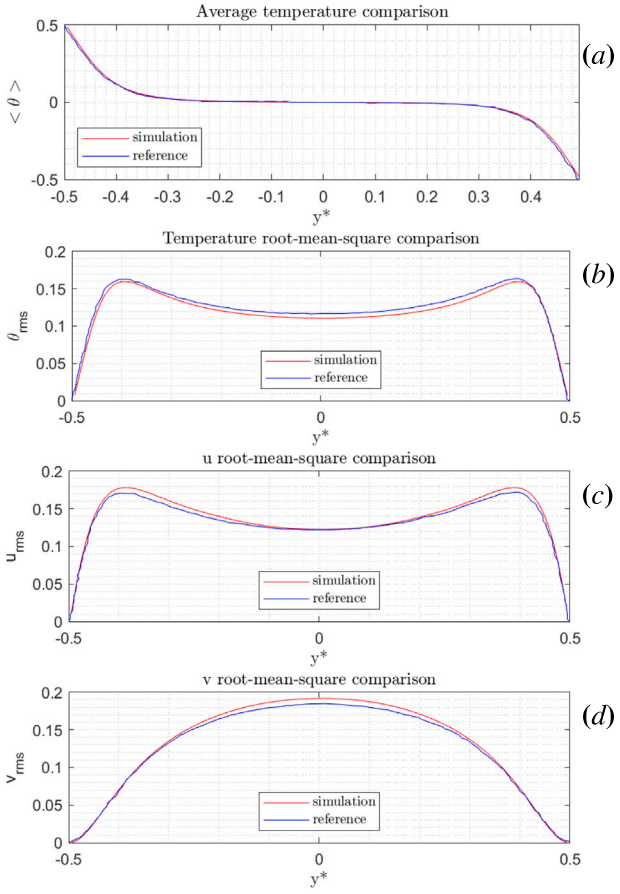

Fig. A.6. Comparison between first- and second-order statistics as obtained by the present numerical method and by Togni et al. [20]: (a) average temperature, (b) root-mean-square temperature, (c) horizontal root-mean-square velocity and (d) vertical root-mean-square velocity.

Data availability

Data will be made available on request.

References

[1] M. Pons, P.L. Quéreé, Modeling natural convection with the work of pressure-forces: A thermodynamic necessity, Internat. J. Numer. Methods Heat Fluid Flow 17 (3) (2007) 322–332, http://dx.doi.org/10.1108/09615530710730184.

[2] A. Barletta, Local energy balance, specific heats and the oberbeck-Boussinesq approximation, Int. J. Heat Mass Transfer 52 (21–22) (2009) 5266–5270, http://dx.doi.org/10.1016/j.ijheatmasstransfer.2009.06.006.

[3] D.D. Gray, A. Giorgini, The validity of the Boussinesq approximation for liquids and gases, Int. J. Heat Mass Transfer 19 (5) (1976) 545–551, http://dx.doi.org/10.1016/0017-9310(76)90168-X.

[4] Z.Y. Zhong, K.T. Yang, J.R. Lloyd, Variable property effects in laminar natural convection in a square enclosure, J. Heat Transf. 107 (1) (1985) 133–138.

[5] J. Hernández, B. Zamora, Effects of variable properties and non-uniform heating on natural convection flows in vertical channels, Int. J. Heat Mass Transfer 48 (3–4) (2005) 793–807, http://dx.doi.org/10.1016/j.ijheatmasstransfer.2004.09.024.

[6] B. Morrone, A. Campo, Influence of intense symmetric heating and variable physical properties on the thermo-buoyant airflow inside vertical parallel-plate channels, J. Heat Transf. 132 (10) (2010) 104501.

[7] S. Ashkenazi, V. Steinberg, High Rayleigh number turbulent convection in a gas near the gas-liquid critical point, Phys. Rev. Lett. 83 (1999) 3641–3644, http://dx.doi.org/10.1103/PhysRevLett.83.3641, URL: https://link.aps.org/doi/10.1103/PhysRevLett.83.3641.

[8] G. Ahlers, F.F. Araujo, D. Funfschilling, S. Grossmann, D. Lohse, Non-Oberbeck–Boussinesq effects in gaseous Rayleigh–Bénard convection, Phys. Rev. Lett. 98 (5) (2007) http://dx.doi.org/10.1103/PhysRevLett.98.054501.

[9] G. Ahlers, E. Calzavarini, F.F. Araujo, D. Funfschilling, S. Grossmann, D. Lohse, K. Sugiyama, Non-Oberbeck–Boussinesq effects in turbulent thermal convection in ethane close to the critical point, Phys. Rev. E - Stat. Nonlinear, Soft Matter Phys. 77 (4) (2008) http://dx.doi.org/10.1103/PhysRevE.77.046302.

[10] M. Macek, G. Zinchenko, V. Musilová, P. Urban, J. Schumacher, Assessing non-Oberbeck–Boussinesq effects of convection in cryogenic helium, Phys. Rev. Fluids 8 (9) (2023) http://dx.doi.org/10.1103/PhysRevFluids.8.094606.

[11] G. Ahlers, X. He, D. Funfschilling, E. Bodenschatz, Heat transport by turbulent Rayleigh–Bénard convection for pr $\simeq$ 0.8 and $3 \times 10^{12} \lesssim$ ra $\lesssim 10^{15}$: aspect ratio Γ = 0.50, New J. Phys. 14 (10) (2012) 103012, http://dx.doi.org/10.1088/1367-2630/14/10/103012.

[12] S. Horn, O. Shishkina, C. Wagner, On non-Oberbeck–Boussinesq effects in three-dimensional Rayleigh–Bénard convection in glycerol, J. Fluid Mech. 724 (2013) 175–202, http://dx.doi.org/10.1017/jfm.2013.151.

[13] X. He, E. Bodenschatz, G. Ahlers, Azimuthal diffusion of the large-scale-circulation plane, and absence of significant non-Boussinesq effects, in turbulent convection near the ultimate-state transition, J. Fluid Mech. 791 (2016) http://dx.doi.org/10.1017/jfm.2016.56.

[14] S. Weiss, M.S. Emran, O. Shishkina, What Rayleigh numbers are achievable under Oberbeck–Boussinesq conditions? J. Fluid Mech. 986 (2024) http://dx.doi.org/10.1017/jfm.2024.389.

[15] X. Chavanne, F. Chillà, B. Castaing, B. Hébral, P. Chabaud, J. Chaussy, Observation of the ultimate regime in Rayleigh–Bénard convection, Phys. Rev. Lett. 79 (19) (1997) 3648–3651, http://dx.doi.org/10.1103/PhysRevLett.79.3648.

[16] J. Boussinesq, Theorie Analytique de la Chaleur, Vol. 2, Gauthier-Villars, Paris, 1903.

[17] G. Ahlers, S. Grossmann, D. Lohse, Heat transfer and large scale dynamics in turbulent Rayleigh–Bénard convection, Rev. Modern Phys. 81 (2) (2009) 503.

[18] R.A. Svehla, Estimated Viscosities and Thermal Conductivities of Gases at High Temperatures, vol. 132, National Aeronautics and Space Administration, 1963.

[19] H. Yik, V. Valori, S. Weiss, Turbulent Rayleigh–Bénard convection under strong non-Oberbeck–Boussinesq conditions, Phys. Rev. Fluids 5 (10) (2020) http://dx.doi.org/10.1103/PhysRevFluids.5.103502.

[20] R. Togni, A. Cimarelli, E. De Angelis, Physical and scale-by-scale analysis of Rayleigh–Bénard convection, J. Fluid Mech. 782 (2015) 380–404.

[21] O. Shishkina, R.J. Stevens, S. Grossmann, D. Lohse, Boundary layer structure in turbulent thermal convection and its consequences for the required numerical resolution, New J. Phys. 12 (7) (2010) 075022.

[22] B.I. Shraiman, E.D. Siggia, Heat transport in high-Rayleigh-number convection, Phys. Rev. A 42 (6) (1990) 3650.